Native 3D Structure of Eukaryotic 80S Ribosome: Morphological Homology with the *E. coli* 70S Ribosome

Adriana Verschoor, Suman Srivastava, Robert Grassucci, and Joachim Frank

Wadsworth Center, New York State Department of Health, Empire State Plaza, Albany, New York 12201-0509

Abstract. A three-dimensional reconstruction of the eukaryotic 80S monosome from a frozen-hydrated electron microscopic preparation reveals the native structure of this macromolecular complex. The new structure, at 38 Å resolution, shows a marked resemblance to the structure determined for the *E. coli* 70S ribosome (Frank, J., A. Verschoor, Y. Li, J. Zhu, R.K. Lata, M. Radermacher, P. Penczek, R. Grassucci, R.K. Agrawal, and S. Srivastava. 1996*b*. In press; Frank, J., J. Zhu, P. Penczek, Y. Li, S. Srivastava, A. Verschoor, M. Radermacher, R. Grassucci, R.K. Lata, and R. Agrawal. 1995. *Nature (Lond.).* 376:441–444.) limited to a comparable resolution, but with a number of eukaryotic elaborations superimposed. Although considerably greater size and intricacy of the features is seen in the morphology of the large subunit (60S vs 50S), the most striking differences are in the small-subunit morphology (40S vs 30S): the extended beak and crest features of the head, the back lobes, and the feet. However, the structure underlying these extra features appears to be remarkably similar in form to the 30S portion of the 70S structure. The intersubunit space also appears to be strongly conserved, as might be expected from the degree of functional conservation of the ribosome among kingdoms (Eukarya, Eubacteria, and Archaea). The internal organization of the 80S structure appears as an armature or core of high-density material for each subunit, with the two cores linked by a single bridge between the platform region of the 40S subunit and the region below the presumed peptidyltransferase center of the 60S subunit. This may be equated with a close contact of the 18S and 28S rRNAs in the translational domain centered on the upper subunit:subunit interface.

ALTHOUGH much less well studied than the *E. coli* 70S ribosome, largely because of its greater complexity and difficulty of preparation, the 80S eukaryotic ribosome shows a great deal of similarity to its eubacterial counterpart. Increases in numbers of components, both ribonucleoprotein (RNP)[1] components and nonribosomal translational factors (for review see Nygard and Nilsson, 1990), are thought to be the result of the need for greater accuracy of the translational process, and tighter regulation of the steps involved in it, but in general the eukaryotic translational process shows strong homology with the eubacterial one.

The eukaryotic ribosome is a highly intricate macromolecular complex. It is significantly larger than the eubacterial ribosome, with a molecular mass of ~4 million daltons, as compared to 2.8 million daltons. Across the kingdom Eukarya, however, the large (60S) subunit is rather variable in size. In plants it is 2.45–2.5 million daltons, while in mammals it may reach 3 million daltons (Bielka, 1982). Some of the size variability of the 60S subunit is due to variation in the size of the 28S rRNA, which ranges from 1.2 to 1.7 million daltons (Bielka, 1982). In contrast, the molecular mass of the small (40S) subunit is fairly constant, ~1.5 million daltons.

In the 40S ribosomal subunit, the consensus 18S rRNA has three notable sequence insertions, as compared to the 16S rRNA of the *E. coli* 30S subunit (e.g., Neefs et al., 1991). The 40S subunit contains ~33 proteins, as compared to 21 in the 30S subunit. The 18S rRNA comprises ~45% of the mass of the subunit. The mammalian 60S subunit contains ~49 proteins (fewer in lower eukaryotes), compared to 34 for the *E. coli* large subunit. It has three rRNAs, the 5S, 5.8S, and 28S rRNAs, compared to the two (5S and 23S) for the *E. coli* 50S subunit. The rRNA moiety comprises ~60% of the mass of the 60S subunit. A striking difference between eubacterial and eukaryotic monomeric ribosomes is in the RNA:protein ratio: the eukaryotic 80S ribosome is only ~60% RNA, while the *E. coli* ribosome is 66% RNA.

One goal of reconstructing the 80S ribosome is to determine the degree of morphological homology of the eukaryotic large and small subunits with the eubacterial

Please address all correspondence to A. Verschoor, Wadsworth Center, New York State Department of Health, Empire State Plaza, P.O. Box 509, Albany, NY 12201-0509. Tel.: (518) 486-4909; Fax: (518) 474-8590. e-mail: adri@orkney.ph.albany.edu

1. *Abbreviations used in this paper*: CTF, contrast transfer function; HAC, hierarchical ascendant classification; PCA, principal components analysis; RNP, ribonucleoprotein.

ones, as well as the degree to which their associations into the monomeric ribosomes are analogous. The extent of the morphological and spatial homology can then give us new insights into the intricate combination of conserved and variable aspects of the protein synthetic process.

Materials and Methods

Ribosomes were isolated from wheat germ according to Montesano and Glitz (1988). Cryo-electron microscopy was performed as described previously (Lepault et al., 1983; Dubochet et al., 1988; Wagenknecht et al., 1988) using a Philips EM420 equipped with a low-dose kit, Gatan cryostage, and cryo transfer device, at 100 kV and a nominal magnification of 36,000 (actual magnification, 34,766). Molybdenum grids covered with holey carbon film were used in an effort to enhance any preference of the ribosomes to assume certain orientations. Grids were two-side blotted, and a guillotine device was used to achieve the freezing. Nontilt micrographs were recorded at a defocus of ~2.0 μm and tilt micrographs with a midfield defocus of ~1.5–1.8 μm. The micrographs were digitized on a PDS1010A microdensitometer with an aperture of 20 μm, resulting in a pixel size of 5.75 Å on the object scale (Perkin Elmer Cetus Corp., Norwalk, CT).

Analysis of the 80S ribosome was by single-particle methods, using the random conical geometric scheme (Radermacher et al., 1987; Frank and Radermacher, 1992). Briefly, pairs of individual particle projections (0 and 50°) are windowed from micrograph pairs, using the interactive particle selection program contained in SPIDER (Frank et al., 1981, 1996*a*). The set of nontilt projections, including all of the views of the particle occurring in the micrographs, is aligned using a reference-free alignment scheme (Penczek et al., 1992), and then subjected to multivariate statistical analysis (MSA), Principal Components Analysis (PCA) or Correspondence Analysis (CA), followed by Hierarchical Ascendant Classification (HAC) (Frank, 1990). Either a weighted back-projection (e.g., Radermacher, 1988) or an iterative back-projection (Penczek et al., 1992) algorithm is used to calculate the 3D reconstruction. Constraints within the iterative algorithm, notably limitation of the minimum and maximum densities, provide a certain amount of internal noise-suppression, before low-pass filtration. The projection set for the full reconstruction is then split, and half-set reconstructions are calculated to determine the resolution by the 3D differential phase residual (PR_{45}) calculation. The full-set reconstruction is then limited to this resolution by Fermi low-pass filtration. Wiener filtration is applied to cryo structures before the step of low-pass filtration, for correction of the contrast transfer function (see below).

A total of 1,892 pairs of individual particle projections encompassing all views attributable to monomeric ribosomes were windowed from four micrograph pairs. After alignment by a reference-free scheme, the 2D resolution of the total set was assessed to be ~27 Å by phase residual analysis.

Hierarchical classification using 119 factors was performed, using complete linkage as the clustering criterion. 136 classes obtained were analyzed by averaging and visual inspection. Fourteen of the classes (27–175 images each) appearing to represent the same view were chosen for further analysis; these contained a total of 918 particle images. Although we expected to be able to identify substantial-membership subsets relating to the several more or less strongly preferred views that had been recognized in earlier negative stain preparations (Nonomura et al., 1971; Lutsch et al., 1972; Verschoor and Frank, 1990), the single view predominated. Yet more unexpectedly, this was not the preferred left-featured frontal view (Nonomura et al., 1971) that was analyzed in our previous negative stain study of the 80S ribosome (Verschoor and Frank, 1990). That highly distinctive view was not recognized in any of the useable HAC classes.

The preferred view found in the cryo-data set represents a significant rotation away from the familiar frontal view (see below). After the 3D reconstruction was obtained, the two orientations were found to be related by an angle of approximately (phi 130°, theta 130, psi 40); for definition of the Eulerian angles, see Radermacher (1991).

The 918 tilt projections corresponding to the HAC set of 0° projections were centered and labeled by tilt and azimuthal angles, and then submitted to an iterative back-projection algorithm. The tilt angles ranged from 43.0 to 53.5°; the great majority were between 49.9 and 50.2°. The alignment of the entire set of 1982 projections was refined using a method in which each projection was correlated to an appropriate projection computed from the reference volume (Radermacher et al., 1987, 1992).

Reconstructions using the aligned projections were computed over the whole set of 1982 and over the HAC set used for the initial reconstruction. Of the various strategies pursued, the best quality reconstruction proved to be that calculated from the refined-aligned HAC set of 918 images; the full-set reconstructions were of markedly poorer quality, due to their inclusion of heterogeneous projection sets. The set of 918 was split, and half-set reconstructions were calculated to give a PR_{45} of 38.3 Å. A Fermi low-pass filter limiting the data to this resolution was applied.

Once a robust reconstruction had been achieved, other methods were investigated in the effort to improve the resolution. A particular effort was made to recognize additional preferred views in the original data set, that could be used for separate reconstructions. This is because refinement by projection matching (Penczek et al., 1994; Radermacher, 1994), in which the original particle images are correlated individually with projections computed from the reconstruction at all possible angles, does not lead to improved resolution in situations where a significant missing cone cannot be compensated (Penczek, P., personal communication). Extensive efforts were made to reduce the missing cone. Further HAC analysis led to the identification of five small groups (containing at least 40 images) representing slightly different views. These were analyzed by computation of 3D reconstructions over each set. As had been apparent from visual inspection of their 0° averages, however, these represented mere rocking positions of the preferred view; they differed in tilt angle by at most −17 to +5°. Nevertheless, the reconstruction was repeated with the addition of 129 projections with recalculated tilt angles of between 50 and 70°. Finally, the restoration method of projection onto convex sets (e.g., Sezan, 1992) was applied to the random conical reconstruction to fill in missing angular information.

Methods to compensate for the effects of the microscope's contrast transfer function, such as Wiener filtration, have been under development in our laboratory (Frank and Penczek, 1994). Correction of the contrast transfer function (CTF) is as yet problematic for a data set of the type used, in which the defocus varies across an entire tilt micrograph. Refinement of the structure from nontilt micrographs recorded at different defoci (Zhu, J., P. Penczek, R. Schröder, and J. Frank, manuscript in preparation) provides a situation in which correction can be applied more precisely. Thus, correction for this 80S structure was approximate. The range of defocus across the regions of the tilt micrographs from which particles were selected was determined. The median defocus was used as a basis for the design of the Wiener filter. The exact shape of the filter function for this type of tilt data has yet to be optimized.

All calculations were performed on a DEC 3000 model 400 Alpha workstation running under VMS. Reconstruction volumes were analyzed and displayed using WEB, the graphical interface of SPIDER and AVS (Advanced Visual Systems, Waltham, MA). AVS was used to compare the 80S morphology with that of the 70S structure recently computed in our laboratory (Frank et al., 1995*a*,*b*) using similar methods. It was also used for visualization of multiple density thresholds. Dual-threshold representations were calculated according to the criterion used by Milligan and Unwin (1986), to enable direct comparison of our (single particle) cryo reconstruction with their (crystalline) cryo reconstruction. Inside the normal density threshold delineating the envelope of the macromolecule, a higher threshold is set, at 25% of the total volume. This level was estimated to enclose roughly 65% of the rRNA, if the simplifying assumption is made that the rRNA and r-protein comprised distinct moieties.

Results

Morphology of the 80S Ribosome

The 80S ribosome from wheat germ was reconstructed by the random-conical method from 918 images derived from four tilt pairs of micrographs (Fig. 1). The strongly preferred view used for the reconstruction was identified by MSA/HAC sorting (Fig. 2). The 80S ribosome reconstruction appears in surface representations (Fig. 3; Fig. 4, *B* and *C*) as an overall globular-to-ellipsoidal structure, with a clear division into a roughly tabular small subunit and a roughly hemiellipsoidal large subunit, separated at the top but in close contact at their lower halves. Even at our moderate (38 Å by PR_{45}) resolution, many features and protrusions are seen on both subunits. The dimensions of the wheat germ ribosome, calculated from the frontal-view orientation are: height 294 Å, width 311 Å, and thickness

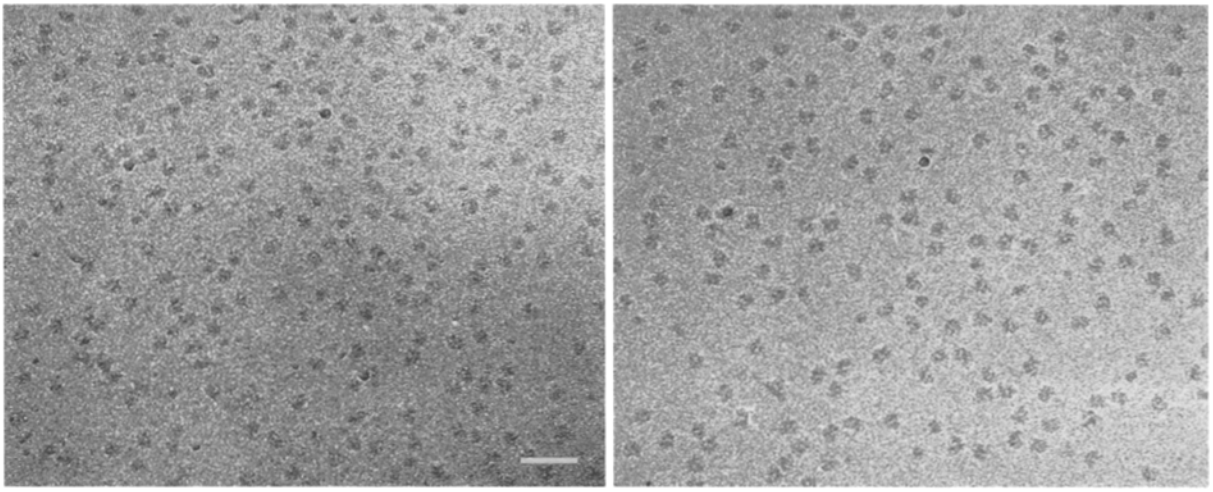

Figure 1. Cryo-electron micrographs of wheat germ 80S ribosomes: portions of tilt (50°) and nontilt (0°) micrograph pair used for 3D reconstruction according to a random conical scheme (see Materials and Methods). Bar, 1,000 Å.

197 Å. The height measurement agrees well with the 296 Å determined for the dissociated 40S subunit (Srivastava et al., 1995).

The 40S Subunit

Both subunits of the 80S structure are characterized by a large number of peripheral protrusions. The 40S subunit has effectively a ridgeline of protruding features: from the blunt beak on the front of the head, to the rather pointed crown of the head, the crest on the back of the head, the upper back lobe of the body, the lower back lobe (which appears in one range of views [Fig. 3, row 1, images 3–5] to actually be two protrusions rather than a single one), and finally the pointed, conical back foot. The interior region bounded by this irregular periphery appears shallowly concave and relatively featureless. Although some of these protrusions were recognized in earlier 2D negative-stain studies (e.g., Frank et al., 1982; Kiselev et al., 1982), their native orientations are in many cases quite different from what was inferred from the negative-stain information. Among the most notable are the trend of the crest and ear, both roughly normal to the trend of the beak, and the marked relief of the front-body lobe (see below).

The 80S structure confirms several recent findings on the morphology of the 40S subunit. In our cryo 3D reconstruction of the dissociated 40S subunit (Srivastava et al., 1995), we distinguished a pronounced platform structure, analogous to the well known platform of the prokaryotic 30S subunit. Morphology-based evolutionary hypotheses in the literature (e.g., Lake et al., 1985), as well as the appearance of these features in our earlier negative-stain reconstructions of the 40S and 80S structures (Verschoor et al., 1989; Verschoor and Frank, 1990; Srivastava et al., 1992), had appeared to suggest that the back lobes represented some type of bifurcated platform. Instead, the cryo studies show us that the back lobes are features essentially independent of the underlying platform structure, which is unexpectedly similar in form to that of the 30S subunit (see below). In our 80S reconstruction, the cup shape of the platform is very distinct.

Another notable finding is the delineation, in cryo preparations, of what we term the frontal lobe, comprising the portion of the small-subunit body that, in the monosome, lies closest to the P-protein stalk of the large subunit (see below). This cylindrical front-body lobe, which appears enrolled like the arm of a fauteuil, shows unexpectedly high relief. Both its top and bottom terminate conically, with the bottom terminal comprising the front foot or basal lobe of the subunit. The "throat" (Srivastava et al., 1992) area above this lobe had been in negative stain, variable in appearance due presumably to stain effects, which may have included a contribution from positive staining of exposed 18S rRNA. The new structure shows it as a thin webbing between beak and subunit body.

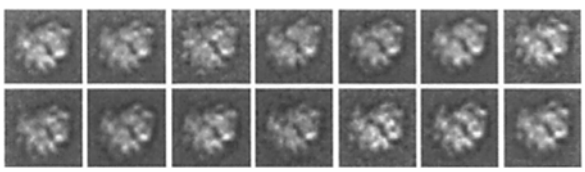

Figure 2. Cluster averages representing sets of projections classified into major groups by MSA and HAC (see Materials and Methods). The tilt counterparts to the sets of projections in these 14 averages, totaling 918 images, were used for the 3D reconstruction.

The 60S Subunit

The 60S large subunit of the 80S structure also reveals an intricate morphology. The consensus large-subunit peripheral features are readily recognizable: the central protuberance (CP), the proximal portion of the P-protein stalk, and a mushroom-shaped arm, that we will term the L1-analogue arm, corresponding to the *E. coli* L1 arm. Although the L1-analogue arm pinches off readily with small changes in the density threshold used for visualization, its distal portion is very persistent.

Rather than being a smooth hemi-ellipsoid, the 60S-subunit body is irregular, with numerous protrusions, bumps,

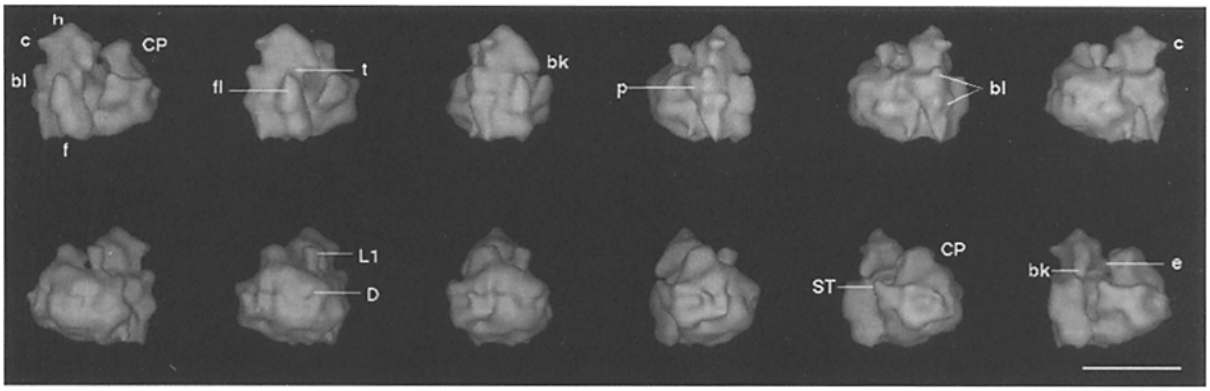

Figure 3. Surface representations (30° rotational increment around vertical axis) of refined cryo 80S 3D reconstruction from 918 particle images. Abbreviations: (40S subunit) *h*, head; *c*, crest; *bl*, back lobes; *f*, feet; *fl*, frontal lobe; *t*, throat; *bk*, beak; *p*, platform; *e*, ear; (60S subunit) *CP*, central protuberance; *L1*, L1-analogue arm; *D*, dimple; *ST*, P-protein stalk. Bar, 250 Å.

and indentations (unresolved holes?). The P-protein stalk is present as a short and strongly tapering arm, curving forward towards the 40S subunit, across the subunit:subunit interface (Fig. 3, row 2, images 4–6). Presumably, this arm represents the proximal portions of some of the elongate P proteins, while the distal portions were sufficiently variable in position among the individual ribosomes in the data set that they blurred out in the 3D reconstruction and are not imaged.

The body structure below the stalk, previously (Verschoor and Frank, 1990) termed the stalk-base ridge, is elaborately developed. The back of the 60S subunit shows a number of bumps and indentations; these will be described in greater detail (see below). The apparent shape of the subunit varies rapidly with small changes in rotation angle, from strongly ellipsoidal (Fig. 3, row 2, images 1–2) to quite globular (Fig. 3, row 2, images 3–4). This accounts for the paradox that the 60S subunit in the 80S ribosome can resemble the 50S structure in the 70S ribosome so closely in the crown orientation (see below), yet be so markedly elongated in a lateral direction in other comparisons to the 50S structure.

Ideally, we would like to be able to compare an individual structure determined for the dissociated 60S subunit to our 80S structure, as we are able to do for the 40S subunit (Srivastava et al., 1995). This would cast further light on, in particular, the details of the interface surfaces of the subunits. However, due to the well known intractability of the 60S subunit as a specimen, the only reconstruction so far achieved in our laboratory (Vickers, W., S. Srivastava, A. Verschoor, and P. Penczek, unpublished results) is at too low a resolution to corroborate such information. Future efforts to reconstruct the 60S subunit will undoubtedly be based on projection matching with the 60S portion of our 80S monosome structure.

Internal Organization: Features of the High-Density Core

Finally, we will briefly survey the internal features of the 80S ribosome structure, as revealed by a dual-threshold representation (see Materials and Methods).

Features visualized at the higher threshold are not definitively identifiable with purely rRNA structures; densely packed ribonucleoprotein or RNP may not be distinguishable from RNA, just as more loosely packed RNP may not be distinguishable from protein. Especially at our moderate resolution, a strict attribution is not defensible. However, the distribution of dense material, which is affected only in detail by variations of the Wiener and Fermi filtrations that were used, leads us to characterize this internal density distribution as representing an internal scaffolding, regardless of its actual composition.

When the two subunits are viewed in the classical frontal view of the 80S ribosome, a two-lobed organization of the high-density material is evident (Fig. 5 *A*), corresponding to the cores of the two subunits. In the 60S lobe, two subregions of high density are seen: the massive lower-body core linked to the 40S core by the bridge feature, and, above a waistlike constriction, a second, upper domain centered on the elongation region, which includes the CP and the entire stalk-base substructure. At high threshold the back of the 60S subunit appears to comprise an arrangement of several crosswise, arching rib structures. A shieldlike area of high density extends from the CP to the stalk-base ridge (Verschoor and Frank, 1990). In contrast, the 40S small-subunit core is thin and elongate. Even at high thresholds, this core shows extensions into the beak, back lobes, and feet, the typical surface features of the 40S subunit (Fig. 5). The head remains strongly connected to the body by a thin neck, in a continuous arrangement of the high-density material.

The subunit cores are joined by a well-defined bridge feature (Fig. 5, *A* and *B*), as was seen in an *E. coli* 70S structure calculated at similar resolution (Frank et al., 1991). It appears to join the recently characterized "platform" region of the 40S subunit (Srivastava et al., 1995) to the interface canyon (IC) region of the 60S subunit. No trace of the P-protein stalk (the eukaryotic analogue of the L7/L12 stalk) is seen at this threshold (Fig. 5, *A* and *B*), although the stalk-base ridge remains a major feature.

Discussion

Several types of comparisons help to place the new 80S structure in context: comparison to a previous negative stain 80S structure at similar resolution; comparison to a

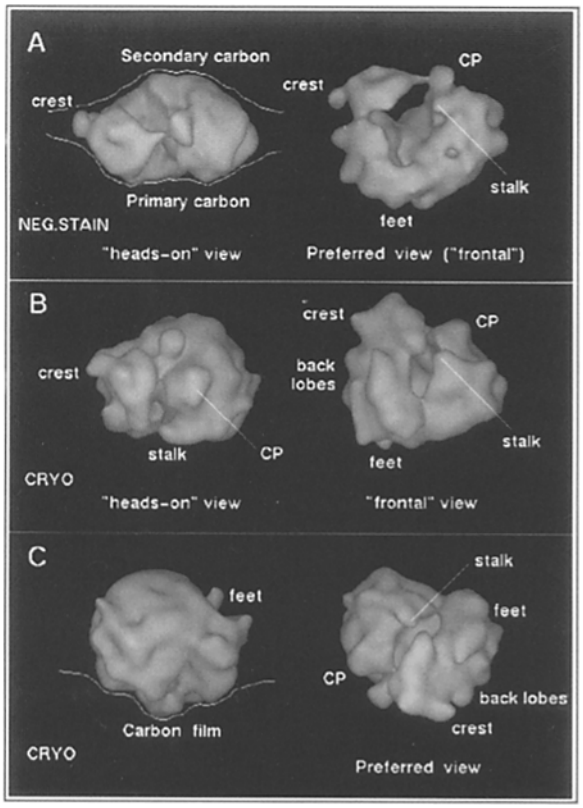

Figure 4. Comparison of negative stain 80S 3D reconstruction from rabbit reticulocyte ribosomes to cryo 3D reconstruction from wheat germ ribosomes. *A* to *B* comparison: morphological comparison; *A* to *C* comparison: specimen geometries. (*A*) Negative stain 3D structure in its preferred orientation, the left-featured frontal view. (*Right panel*) Surface representation corresponding to 0° projection. (*Left panel*) Highly schematic interpretation of deformation of ribosome structure through wrapping (Kellenberger et al., 1982) of the two carbon films of the carbon sandwich. The degree of 'cocooning' by the two 50-Å thick carbons (drawing not to scale) has been exaggerated for simplification. The lines drawn can be considered to represent the absorptive surfaces of the two carbon films. The primary carbon (Verschoor et al., 1986) is the carbon to which the particle originally adsorbed; the secondary carbon is the sandwiching carbon applied to the opposite side of the particle-stain preparation. (*B*) Cryo 3D structure in orientations analogous to the negative stain views in *A*. (*Right panel*) 80S viewed in roughly frontal orientation. Some of the marked difference in the 'openness' of the intersubunit space may be due to the existence of positive staining effects in the negative stain structure. (*Left panel*) View analogous to the "heads-on" view in *A*, showing the much more globular form of the ribosome in the absence of negative staining and air drying. (*C*) Cryo 3D structure in its preferred orientation. (*Right panel*) Surface representation corresponding to 0° projection. (*Left panel*) Schematic of adsorption of 80S particle to carbon in cryo preparation. The deformation of the carbon has again been exaggerated. The lack of collapse of the structure, compared to the image in *A*, is clear. In *C*, the direction of the missing cone, with incomplete information, is in the front-to-back or z-direction, from the beak of the 40S-subunit head to the subunit bases. Abbreviations: *CP*, central protuberance of 60S subunit; *stalk*, P-proteins stalk of 60S subunit; *feet*, feet or basal lobes of 40S subunit; *back lobes*, back lobes of 40S subunit; *crest*, crest feature of head of 40S subunit.

lower-resolution cryo 80S structure from 2D crystals; and comparison to a cryo structure for the 70S *E. coli* ribosome. The former two comparisons will consider what new information our 80S structure reveals about the eukaryotic ribosome; the latter comparison will shed light on the extent of interkingdom homology and conservation of ribosome structure.

Finally, we will suggest a structural basis for some of the morphological features of the new 80S structure, in particular, for the small ribosomal subunit. Our findings support the validity of hypotheses concerning the morphological similarity of eubacterial and eukaryotic ribosomes.

Comparison to Negatively Stained 80S Ribosome Reconstruction

The reconstructed 80S ribosome from wheat germ shows obvious resemblance (Fig. 4) to the earlier negative stain structure for the 80S ribosome from rabbit reticulocytes (Verschoor and Frank, 1990), although several limitations to a direct comparison exist. These include effects of negative stain; source of ribosomes; and difference in the direction of missing information (see legend, Fig. 4 *C* and Materials and Methods).

The much more globular form of the cryo structure supports our earlier (Verschoor, 1989) inference that the negative stain structure may have suffered collapse on the order of 20% in a direction perpendicular to the plane of the carbon support (Fig. 4, *A* and *C*). As noted earlier, the 60S subunit from a mammalian source may actually be 20% larger than that from a higher plant. Because of the deformations in our negatively stained mammalian structure, however, we would not speculate where in the subunit this increase in molecular mass is reflected, relative to the cryo plant structure.

Perhaps the largest discrepancy between the negative stain and cryo structures is in the apparent amount of intersubunit separation, and the openness of the translational domain on the 60S stalk—40S beak side of the ribosome, in the negative stain structure (Fig. 4, *A* and *B*). Inundation of the thin neck region of the 40S subunit, as well as evident stain accumulation in the IC region of the 60S subunit, may explain this discrepancy.

Aside from these reservations, however, good agreement of the two structures is seen in terms of the features of the two subunits. We consider both structures in the classical frontal rotation. Although this was not the preferred orientation in the cryo preparation (see Materials and Methods), it lends itself well to description, as a view in which both subunits are also recognized in classical views: the 40S subunit in lateral view, and the 60S in kidney view.

The 60S subunit in both structures shows similarity of the CP, the proximal portion of the stalk, the stalk-base ridge, and the overall kidney form. The 40S subunit shows good agreement of the back lobes and feet of its body, and the crest feature. The orientation of the crest (Verschoor and Frank, 1990) on the "back" of the 40S head agrees in the negative stain and cryo structures; it juts out in a direction orthogonal to the trend of the beak. The distinctive beak feature was poorly resolved in the negatively stained structure, whereas the cryo structure shows the beak as a

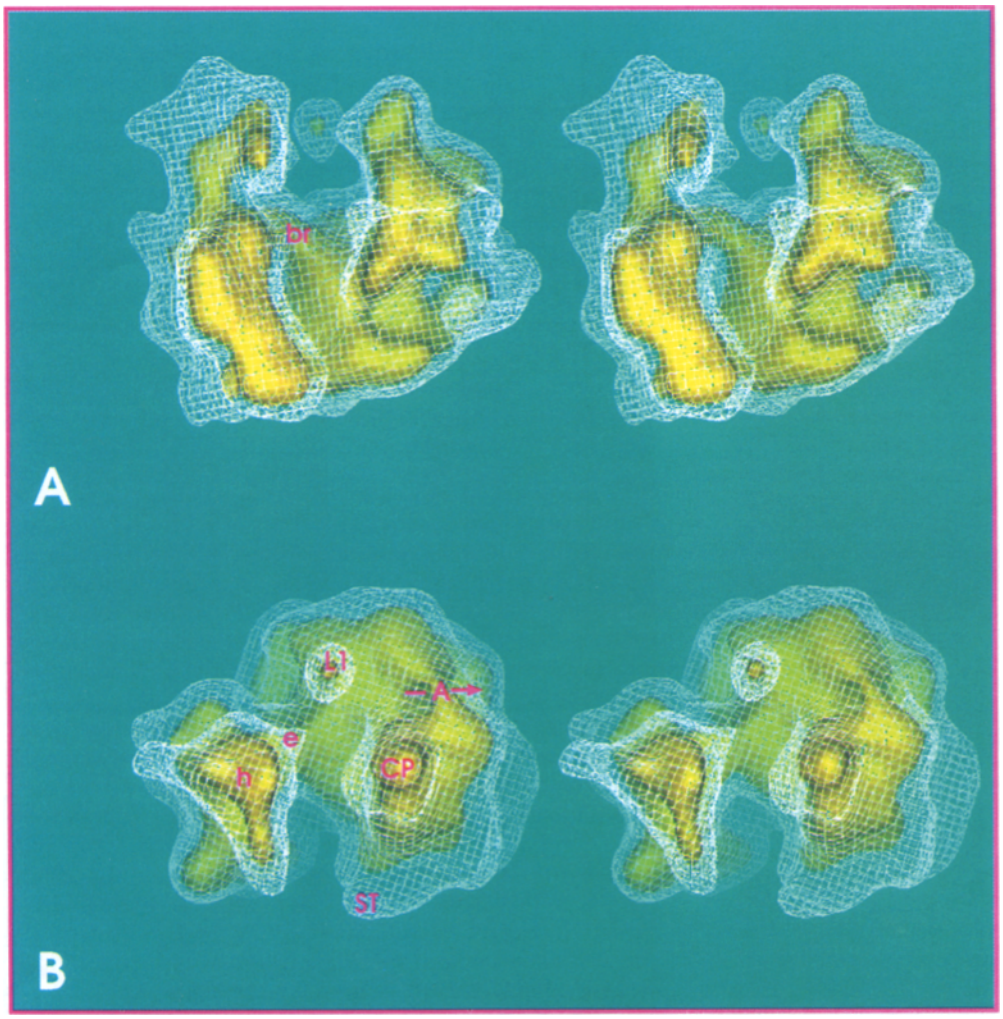

Figure 5. Features of 80S ribosome reconstruction at two density thresholds, in stereo representation. The normal envelope threshold is shown as a white net. The inner, so-called rRNA threshold, visualized as a yellow surface, was set in accord with the convention used by Milligan and Unwin (1986); see Materials and Methods. (*A*) Bilobed organization of the high-density 'core' of the ribosome. Bridge feature (*br*) connects the interface surfaces of the 40S subunit (*left*) and the 60S subunit (*right*). (*B*) Heads-on view (i.e., viewed from the top; rotated 90° around horizontal axis with respect to *A*) of 80S ribosome, showing lower-density "channel" feature, marked by an arrow, extending from PTC region between CP (*CP*) and L1-analogue arm (*L1*) to possible exit site in middle of 60S subunit back. This point of emergence is marked by a deep dimple (cf. Fig. 6 *A*) at normal threshold. The channel passes under a small-diameter upper rib or arch feature (*A*). Other abbreviations: *h*, 40S subunit head; *e*, 40S subunit ear.

well-expressed feature trending parallel to the plane of the subunit:subunit interface, and pointing past the P-protein stalk. In the negatively stained structure a thin bridge appeared to connect the two subunit heads. The cryo structure shows a similarly oriented feature that may or may not correlate with this bridge. The cryo 40S-subunit head has a marked "ear," extending towards the 60S subunit, and roughly coplanar with the crest feature on the opposite, cytoplasmic side of the head.

Comparison to Cryo Reconstruction from Crystals; Features of the Exit Domain

The other comparison that is warranted is with the 80S structure of Milligan and Unwin (1986), computed at lower resolution from chick oocyte ribosome crystals. To facilitate the comparison, a high-density threshold was set for our structure in analogy with that used in the representation of their 3D volume by Milligan and Unwin (1986), at 25% of the volume—a level which they estimated would comprise 65% of the rRNA, if the RNP components were completely partitioned.

The high-density distribution in the crystalline reconstruction appeared in one orientation as a toroid pierced by a small off-center hole, and in the opposite (180°-rotated) orientation as a bilobed form. One lobe appeared globular and the other smaller and elongate, and they were joined or continuous at one end. The hole was inferred to be an exit tunnel. (We note, however, that at the 55-Å resolution of the crystalline structure, it would not be expected to resolve a 20-Å diameter tunnel [see Frank et al., 1996*b*; Stark et al., 1995 for discussions of this point].) In contrast, in the bilobed organization of our structure, the lobes represent the cores of the two subunits, linked in the middle—rather than at one end—by the intersubunit bridge (Fig. 5; cf. Fig. 6 *C*). The open space between the two lobes is simply the intersubunit space. Putative exit features (see below) are oriented roughly perpendicular to the trend of the plane of the subunit:subunit interface. These observations, combined with the results of an earlier 2D analysis of cryo images of tetramers derived from crystalline ribosome sheets (Verschoor et al., 1990), suggest that a change in the assignments made for the subunit positions in the crystalline model would result in a reasonable agreement.

Does our structure contain features suggestive of an exit tunnel? A two-threshold representation in which the two subunits are seen from the top, with the 40S head and 60S CP towards the viewer (Fig. 5 *B*) shows an apparent conduit through the high-density material comprising the 60S-subunit core. This conduit or channel extends from the

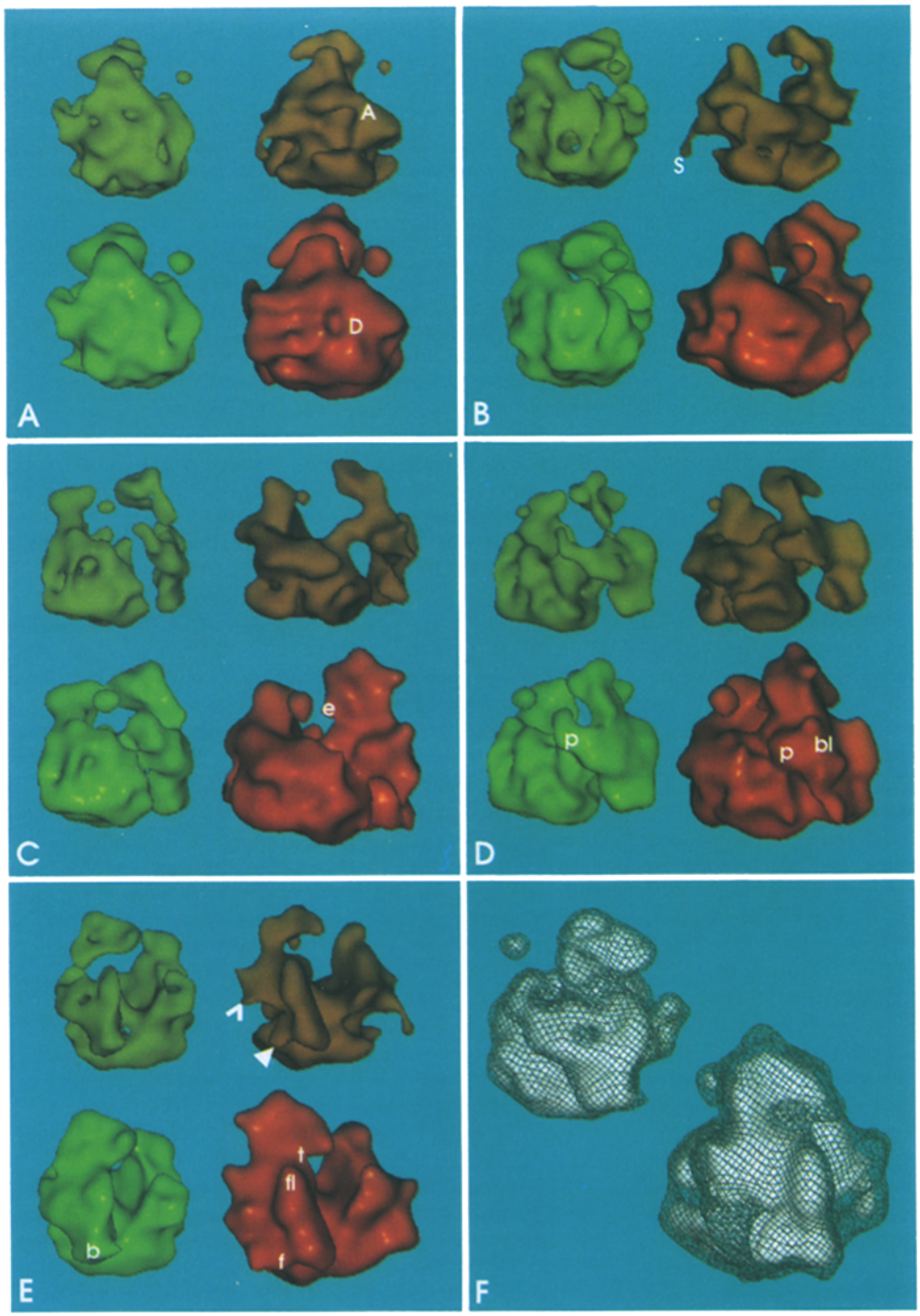

Figure 6. Comparison of cryo 80S and cryo 70S structures at dual thresholds (see Fig. 5). (*A–E*) The 80S structure, to the right in each panel, is depicted in red, with its high-threshold core above in orange. The 70S structure, to the left in each panel, of Frank et al. (1995*a*,*b*), low-pass filtered to comparable resolution, is in green, with its core above in olive. Abbreviations: (small subunit) *p*, platform; *bl*, back lobes, *b*, base; *f*, feet; *fl*, frontal lobe; *t*, throat; *e*, ear; (large subunit) *D*, dimple; *A*, upper back arch or rib; *S*, spike. (*A*) View of the backs of the large subunits, showing the markedly ellipsoidal skiff shape of 60S subunit (Nonomura et al., 1971) vs the globular 50S form. This view suggests that the increase in number of proteins in the 60S structure relative to the 50S structure could result in the lateral broadening of the subunit. (*B*) Intermediate view showing hole and tunnel features in the backs of large subunits. Structures have been rotated by 45° around vertical axis, with respect to *A*. (*C*) View in which small subunits (40S, 30S) are seen platform-on, and large subunits (60S, 50S) are in the classical kidney view. Differences are seen in the platform rim and other features of this aspect of the small subunits, including the back foot region. Structures have been rotated by 90° around vertical axis, with respect to *B*. (*D*) View 45° rotated from *C*, showing another platform-on view of the small subunits, but rotated so that the back lobes of the 40S subunit face more towards the viewer. Structures have been rotated by 45° around vertical axis, with respect to *C*. (*E*) View in which subunits are seen semi-overlapped: the classical frontal view of the 80S ribosome and corresponding view of 70S ribosome. The 40S subunit is in its classical lateral view. This view highlights the eukaryotic elaborations on the 40S subunit, with respect to the 30S subunit. Structures have been rotated by 90° around vertical axis, with respect to *D*. Arrowheads indicate features of the 40S-subunit core not seen in the 30S-subunit core: *filled arrowhead*, back foot core; *open arrowhead*, back lobe core. (*F*) View with small subunits towards viewer, overlapping the large subunits behind. The normal envelope of the structure is depicted as a net, and the high-density core as the solid structure within. In the basal regions of both the 40S and 60S subunits, regions empty of high density material can be seen; these are not seen in the two eubacterial subunits.

presumptive peptidyltransferase (PTC) region to the back of the subunit, under a rib or arch of high density material. (In analogy to the *E. coli* structure, the PTC is considered to be sited on the upper interface aspect of the 60S subunit, below the CP; e.g., Stöffler et al., 1980.) The locations of the two ends of this channel feature agree closely with the two clusters of antibody-binding sites—one at the PTC, and one at mid-back—denoting the location of the

NH_2-terminal of the nascent chain on the 70S ribosome, as determined by Ryabova and coworkers (1988).

At normal threshold, there is a deep dimple in the middle of the back of the 60S subunit in our 80S structure (see below). Its placement coincides with the end of the low-density channel feature, and appears to represent its site of emergence on the surface of the 60S subunit. This lower-density channel feature may thus represent a tunnel, not fully resolved at our current resolution.

Comparison to Cryo E. coli Reconstruction

The existence of structures for the eubacterial and eukaryotic ribosomes obtained by similar methods means that it is for the first time possible to compare the structures of taxonomically divergent ribosomes, and to begin to assess the extent of structural homology or conservation. The new 80S structure was compared to a recent *E. coli* 70S structure (Frank et al., 1995, 1996*b*), filtered to a comparable resolution (Fig. 6).

The broad functional domains defined for the *E. coli* ribosome (e.g., Stöffler et al., 1980; Bernabeau and Lake, 1982) can be recognized through their encompassing of certain morphological features. Much of the delineation of such domains resulted from site mapping experiments, which to a large extent have not been carried out for the eukaryotic ribosome. Two notable exceptions are the mapping of the exit site for both eubacterial and eukaryotic ribosomes by Bernabeau and coworkers (1983), and the mapping of the site of the P-site anticodon-codon interaction (Oakes et al., 1987; cf. Ciesiolka et al., 1985).

Because of the considerable functional conservation of the ribosome, we expect to be able to demarcate similar functional domains on the eukaryotic ribosome as have been described for the eubacterial system. These domains should be spatially delineated by analogous structures, serving largely analogous functions. Where the two ribosomes diverge functionally, e.g., where the eukaryotic ribosome is known to have additional functions (such as the many mechanisms to enhance translational fidelity), the structural basis is not established well enough that we can seek associated featural differences. Here we will confine our attention to a few of the homologous features delineating the translational, elongation, and exit domains or regions, respectively, centered on the intersubunit gap, the (large-subunit) stalk-(small-subunit) front lobe region of the interface, and the mid- to lower back of the large subunit.

The eukaryotic ribosome from a higher plant, wheat, is strongly ellipsoidal, unlike the eubacterial ribosome. Views in which the backs of the large subunits of the two ribosomes are toward the viewer (Fig. 6 *A*) show the significant increase in width of the large subunit: the 60S subunit appears as if stretched, with the same topographic features present, but separated by greater lateral distances. The maximal "stretching" effect and ellipticity of the 60S subunit relative to the 50S subunit is seen with further rotation (Fig. 6 *B*). However, even at angles (e.g., Fig. 6 *A*) where the shape of the 60S subunit diverges dramatically from the globular 50S subunit, we can still recognize that the corresponding morphological features of both subunits remain in register.

For the large subunits the three characteristic protuberances are the CP, the P-protein (or L7/L12) stalk, and the L1-analogue (or L1) stalk. The CPs are similar in the 70S and 80S structures, although in the 70S structure the feature is directed more toward the head of the small subunit (Fig. 6 *C*).

The stalk of the 70S subunit is resolved as a slightly more extended feature, with a somewhat pincer-like morphology, and it persists as a feature at high threshold (Fig. 6 *E*). In the 80S structure, the stalk tapers to a simple point, and shows no persistence at high threshold (i.e., it lacks a dense core), consistent with the fact that the stalk is composed solely of r-proteins.

The appearance of the L1 or L1-analogue arm agrees closely in the eubacterial and eukaryotic structures. Although in previous negative-stain data for both the 50S subunit and 70S ribosome the L1 arm appeared as a long thin, labile feature, this arm in cryo preparations is visualized as a detached bleb. In both the eubacterial and eukaryotic cryo structures, at an envelope threshold that depicts the rest of the ribosome structure well, the L1 or L1-analogue arm pinches off, leaving a floating balloon-shaped feature that represents its tip.

At high threshold, there is a notable absence of dense material in the back of the 60S subunit, on its stalk-wards side (Figs. 5 *A*, 6, *E–F*): a large, horizontally trending notch in the back of the 60S subunit core causes it to have a strongly waisted appearance, between the upper shield-like area and the lower rib. The whole region below and behind the massive stalk-base ridge is empty, except for a single, thin, downwardly pointing dense spike (Fig. 6 *E*). Such "empty" regions are not obvious in the 70S ribosome in an analogous view (Fig. 6, *E* and *F*). One other notable difference is in the presence in the middle of the 60S-subunit back, above the basal notch, of a large, centrally placed dimple, representing the surface expression of a linear feature of lower density (see above) extending through the 60S subunit. This dimple is less marked in the 50S structure, although at the high threshold one of several holes is similarly sited (Fig. 6, *A* and *B*). Another recent *E. coli* ribosome reconstruction (Stark et al., 1995) also shows a low-density pathway from PTC to mid-back, under an upper rib or arch not unlike that in our 80S structure. Due to the lack of CTF correction of this latter structure, however, we must interpret the resemblance with caution.

Although the 60S subunit viewed directly from the back appears much wider than the 50S subunit of the 70S structure, the two large subunits appear virtually identical when viewed from the side, in the classic kidney orientation (Fig. 6 *C*). Both show a rather flat interface profile, joined to the small subunit in the middle of the ribosome by a massive bridge structure. In the 80S structure, there is an additional joining of the two subunits at the base, most likely due to the incomplete angular information.

For comparison of the small-subunit morphologies, the view in Fig. 6 *C* is also particularly interesting. The platform is towards the viewer, and the divergences of the two structures are most clearly seen. In the 70S structure the lip of the platform rises higher and curls more strongly (see also Fig. 6, *D* and *F*). In the 80S structure the superimposition of the two back lobes on the platform results in a markedly different appearance. One back lobe is set high, so that it seems to comprise part of the rim of the cupping

platform. The lower lobe forms a marked bulge below it, about midway down the subunit body. The differences seen initially in the platform region in the 70S and 80S structures partially disguise the fact that homologous platform structures do exist in the two. In the eukaryote the two back lobes merely superimpose on it, rather than substituting for it.

The back foot of the 40S subunit has no counterpart in the eubacterial 30S structure. In an orientation in which the platform faces the viewer (Fig. 6 *D*), the back foot of the 40S subunit appears as a narrow linear feature below the two back lobes. In the 30S subunit, the structure tucks in below the platform, and the subunit base is roughly cylindrical. If the structures are rotated around a vertical axis by 90° (Fig. 6 *E*; see also Fig. 6 *F*), the differences in the subunit bases are seen maximally. This classic lateral view of the 40S subunit in the 80S structure shows all of the peripheral eukaryotic elaborations: the crest and beak of the head, and the back lobes and feet of the body. Although the 30S-subunit in the 70S structure shows at least vestigial expressions of several of these features, such as a strongly twisted, stubby beak (cf. Stark et al., 1995 for knobbed morphology of 30S-subunit beak[2]), and a small bulge approximating the lower back lobe, the eukaryotic back foot has no counterpart whatsoever. The lack of homology in this particular region is borne out when the structures are examined at high density threshold (see below).

In summary, it is clear that although certain features show characteristic differences, overall, the eubacterial and eukaryotic ribosomes have much in common.

Tentative Identification of Several Regions of the 18S rRNA

The cores of the subunits, in both the eubacterial and eukaryotic ribosome structures, are composed of relatively high density material. As discussed above, we are not able to strictly attribute to these dense cores, or internal scaffolds, a purely rRNA composition. However, if for heuristic purposes, we do equate this scaffolding with the deduced organization of the rRNA within the ribosomal subunits, then several interesting points emerge that are consistent with the burgeoning recent models of rRNA tertiary structure and with findings on the quaternary organization of the rRNA and r-proteins. Here we will consider mainly the small subunit with its single rRNA. There is considerable confidence in the validity of the secondary structure models of the 16S and 16S-like (e.g., 18S) rRNAs, derived from extensive phylogenetic comparisons (Konings and Gutell, 1995). Although a well-anchored tertiary structure model for the 18S rRNA lies in the distant future, a certain amount of speculation may be permissible.

When the 3D reconstruction is viewed so that a lateral view of the 40S subunit is seen (Fig. 6, *E* and *F*), the characteristic eukaryotic profile of the subunit is most exaggerated. At the high threshold the beak forms a long curved hook, and the "feet" of the normal-threshold 40S form are echoed by a two-footed appearance of the core. The feet of the dense core are concentrated towards the front of the subunit base, leaving the whole region from lower back lobe to back foot strikingly empty. The most notable feature is the extreme angulation of the upper-body core (Fig. 6 *E*), imparting a major bend or kink in what initially appears as the rather linear form of the 40S subunit, and echoing the morphological importance of the platform feature in the 40S subunit. The subunit neck contains a core of dense material, probably identifiable with an extended region of the 18S rRNA, joining the head and body of the subunit.

It is instructive to examine the patterns of dense material seen in light of the speculations on eukaryotic differences from the eubacterial structure. Lake and coworkers (1982) were interested in determining whether the non-eubacterial "additions"—including the so-called archaebacterial bill, or beak, and the so-called eukaryotic lobes, or feet—were composed principally of rRNA or r-protein. Lake and coworkers (1982) inferred that the feet could contain up to 300 nucleotides of rRNA, which could correspond to one or more of the eukaryotic sequence inserts. In contrast, the beak, from the fact that immunoelectron microscopy showed several proteins to map to this feature, was concluded by Lake and coworkers (1982) to be likely composed primarily of protein.

Relative to the 16S RNA of the 30S subunit, the 18S RNA of the 40S subunit has several insertions in the primary sequence, which map to widely separated regions in the secondary structure (e.g., Neefs et al., 1991; Gutell, 1994). The size of the 18S rRNA from higher plants is very similar to that for yeast, close to 1,800 nt, compared to 1,542 nt for *E. coli*. Thus, the 18S tertiary structure must accomodate ~260 nt more than the 16S structure. Is there any correspondence between the expected tertiary-structure locations for these insertions and any of the high-threshold internal features that we see in our structure for the 40S subunit but not in the 30S subunit structure?

In two of the main regions of difference between the 16S and 18S rRNA secondary structures (Neefs et al., 1991; Gutell, 1994), the 18S sequence shows insertions in the vicinity of helices 10 and 21 (consonant with the 16S rRNA numbering scheme of Brimacombe, 1992). Thus, we would predict that the most likely regions to identify visible local enlargements of the rRNA in the 40S subunit relative to the 30S subunit would be in the regions where helices E21 and E10 are mapped. Can we predict these regions by extrapolating from the tertiary structure models of the *E. coli* 16S rRNA?

The tertiary structure model of the 16S rRNA (e.g., Brimacombe, 1992), when "cross-referenced" with the secondary structure model for the 18S rRNA from a higher plant (Gutell, 1994), indeed shows placements for the eukaryote-specific helices that appear consistent with the distribution of higher-density material in our 40S-subunit structure. The model places helices 10 and 21 in the base of the 30S subunit. Thus, if we assume an analogous mapping of these conserved helices in the 18S rRNA to the base of the 40S subunit, the eukaryotic inserts E10 and E21 should map to adjacent regions. The large E21 insertion could form the strikingly rodlike core of the back foot

2. The beak appears to be a rather labile feature (e.g., Verschoor and Frank, 1990). While the present wheat germ ribosome reconstruction shows it as an extended feature, a recent structure from yeast ribosomes (Verschoor, A., J. Warner, and J. Frank, manuscript in preparation) reveals a twisted morphology, more consistent with that seen in the 40S structure (Srivastava et al., 1995) as well as the *E. coli* 70S structures.

of the 40S subunit. The E10 insert could contribute to the increase in size of the front foot, the main core of the small-subunit base (Fig. 6, *E* and *F*).

One other region contains high density material that may possibly be equated to a specific portion of the 18S rRNA, namely, the intersubunit bridge. Base pairing has been postulated to occur (e.g., Azad, 1979) between two regions near the 3′ ends of the 18S rRNA of the 40S subunit and the 5S rRNA of the 60S subunit. In vitro hybridization takes place readily, and the complex is unusually stable. An analogous phenomenon occurs with the *E. coli* 16S and 5S rRNAs, which show similar sequence complementarity in a strongly conserved region. Reversible conformational changes in the two subunits, causing these regions of their rRNAs to become single stranded as well as surface accessible, and thus able to interact with one another, might be responsible for mediation of subunit association and dissociation. Since, by analogy with the 30S subunit morphology, the 3′ end of the 18S rRNA would be exposed on the interface side of the subunit in the region of the platform, the complementary sequence of the 5S rRNA might be expected to map to the interface aspect of the 60S subunit "across from" this location. Since the intersubunit bridge, with its high-density core, links the two subunits between the interface aspect of the 40S subunit's platform and the lower margin of the 60S subunit's IC (Fig. 5, *A* and *B*), the identification of the posited intersubunit rRNA interaction with this striking morphological feature appears plausible.

We thank Michael Radermacher for extensive computations and for discussions, and Pawel Penczek for assistance with computations and for discussions.

We acknowledge support from National Institutes of Health (R01 GM29169 to J. Frank) and National Science Foundation (BIR 9219043 to J. Frank). We acknowledge extensive use of the Research Computing Core, and also assistance from the Computational Molecular Biology Core, of the Wadsworth Center.

Received for publication 13 October 1995 and in revised form 26 January 1996.

References

Azad, A.A. 1979. Intermolecular base-paired interaction between complementary sequences present near the 3′ ends of 5S rRNA and 18S (16S) rRNA might be involved in the reversible association of ribosomal subunits. *Nucleic Acids Res.* 7:1913–1929.

Bernabeau, C., and J.A. Lake. 1982. Nascent polypeptide chains emerge from the exit domain of the large ribosomal subunit: immune mapping of the nascent chain. *Proc. Natl. Acad. Sci. USA.* 79:3111–3115.

Bernabeau, C., E.M. Tobin, A. Fowler, I. Zabin, and J.A. Lake. 1983. Nascent polypeptide chains exit the ribosome in the same relative position in both eucaryotes and procaryotes. *J. Cell Biol.* 96:1471–1474.

Bielka, H., editor. 1982. The Eukaryotic Ribosome. Springer Verlag, Berlin. 338 pp.

Brimacombe, R. 1992. Structure-function correlations (and discrepancies) in the 16S ribosomal RNA from *Escherichia coli. Biochimie.* 74:319–326.

Ciesiolka, J., K. Nurse, J. Klein, and J. Ofengand. 1985. Conservation of RNA sequence and cross-linking ability in ribosomes from a higher eukaryote: photochemical cross-linking of the anticodon of P site bound tRNA to the penultimate cytidine of the UACACACG sequence in *Artemia salina* 18S rRNA. *Biochemistry.* 24:3233–3239.

Dubochet, J., M. Adrian, J.-J. Chang, J.-C. Homo, J. Lepault, A.W. McDowall, and P. Schultz. 1988. Cryo electron microscopy of vitrified specimens. *Quart. Rev. Biophys.* 21:129–132.

Frank, J. 1990. Classification of macromolecular assemblies studied as 'single particles.' *Quart. Rev. Biophys.* 23:281–329.

Frank, J., and P. Penczek. 1994. On the correction of the contrast transfer function in biological electron microscopy. *Optik.* 98:125–129.

Frank, J., and M. Radermacher. 1992. Three-dimensional reconstruction of single particles negatively stained or in ice. *Ultramicroscopy.* 46:241–262.

Frank, J., B. Shimkin, and H. Dowse. 1981. SPIDER—a modular software system for electron image processing. *Ultramicroscopy.* 6:343–358.

Frank, J., A. Verschoor, and M. Boublik. 1982. Multivariate statistical analysis of ribosome electron micrographs: L and R lateral views of the 40S subunit from HeLa cells. *J. Mol. Biol.* 161:107–137.

Frank, J., P. Penczek, R. Grassucci, and S. Srivastava. 1991. Three dimensional reconstruction of the 70S *Escherichia coli* ribosome in ice: the distribution of ribosomal RNA. *J. Cell Biol.* 115:597–605.

Frank, J., J. Zhu. P. Penczek, Y. Li, S. Srivastava, A. Verschoor, M. Radermacher, R. Grassucci, R.K. Lata, and R. Agrawal. 1995. A model of protein synthesis based on cryo-electron microscopy of the *E. coli* ribosome. *Nature (Lond.).* 376:441–444.

Frank, J., M. Radermacher, P. Penczek, J. Zhu, Y. Li, M. Ladjadj, and A. Leith. 1996*a*. SPIDER and WEB: processing and visualization of images in 3D electron microscopy and related fields. *J. Struct. Biol.* 116:190–199.

Frank, J., A. Verschoor, Y. Li, J. Zhu, R.K. Lata, M. Radermacher, P. Penczek, R. Grassucci, R.K. Agrawal, and S. Srivastava. 1996*b*. A model of the translational apparatus based on three-dimensional reconstruction of the *E. coli* ribosome. *In* Frontiers In Translation. A.T. Matheson, editor. In press.

Gutell, R.R. 1994. Collection of small subunit (16S- and 16S-like) ribosomal RNA structures. *Nucleic Acids Res.* 22:3502–3507.

Kellenberger, E., M. Häner, and M. Wurtz. 1982. The wrapping phenomenon in air-dried and negatively stained preparations. *Ultramicroscopy.* 9:139–150.

Kiselev, N.A., Y.Va. Stel'mashchuk, E.V. Orlova, M. Platzer, F. Noll, and H. Bielka. 1982. On the fine structure of rat liver ribosome small subunits. *Mol. Biol. Rep.* 8:185–189.

Konings, D.A.M., and R.R. Gutell. 1995. A comparison of thermodynamic foldings with comparatively derived structures of 16S and 16S-like rRNAs. *RNA.* 1:559–574.

Lake, J.A., E. Henderson, M.W. Clark, and A.T. Matheson. 1982. Mapping evolution with ribosome structure: intralineage constancy and interlineage variation. *Proc. Natl. Acad. Sci. USA.* 79:5948–5952.

Lake, J.A., M.W. Clark, E. Henderson, S.P. Fay, M. Oakes, A. Scheinman, J.P. Thornber, and R.A. Mah. 1985. Eubacteria, halobacteria, and the origins of photosynthesis: the photocytes. *Proc. Natl. Acad. Sci. USA.* 82:3716–3720.

Lepault, J., F.P. Booy, and J. Dubochet. 1983. Electron microscopy of frozen biological suspensions. *J. Microsc.* 129:89–102.

Lutsch, G., H. Bielka, K. Wahn, and J. Stahl. 1972. Studies on the structure of animal ribosomes. III. Electron microscopic investigations of isolated rat liver ribosomes and their subunits. *Acta Biol. Med. Germ.* 29:851–876.

Milligan, R.A., and P.N.T. Unwin. 1986. Location of exit channel for nascent protein in 80S ribosome. *Nature (Lond.).* 319:693–695.

Montesano, L., and D.G. Glitz. 1988. Wheat germ cytoplasmic ribosomes: structure of ribosomal subunits and localization of N6,N6-dimethyladenosine by immunoelectron microscopy. *J. Biol. Chem.* 263:4932–4938.

Neefs, J.-M., Y. Van de Peer, P. De Rijk, A. Goris, and R. De Wachter. 1991. Compilation of small ribosomal subunit RNA sequences. *Nucleic Acids Res.* Vol 19. Suppl., pp. 1987–2015.

Nonomura, Y., G. Blobel, and D. Sabatini. 1971. Structure of liver ribosomes studied by negative staining. *J. Mol. Biol.* 60:303–323.

Nygard, O., and L. Nilsson. 1990. Translational dynamics: interactions between the translational factors, tRNA and ribosomes during eukaryotic protein synthesis. *Eur. J. Biochem.* 191:1–17.

Oakes, M., A. Scheinman, M. Rivera, D. Soufer, G. Shankweiler, and J. Lake. 1987. Evolving ribosome structure and function: rRNA and the translation mechanism. *Cold Spring Harbor Symp. Quant. Biol.* II:675–685.

Penczek, P., M. Radermacher, and J. Frank. 1992. Three-dimensional reconstruction of single particles embedded in ice. *Ultramicroscopy.* 40:33–53.

Radermacher, M. 1988. Three-dimensional reconstruction of single particles from random and nonrandom tilt series. *J. Elec. Microsc. Tech.* 9:359–394.

Radermacher, M. 1991. Three-dimensional reconstruction of single particles in electron microscopy. *In* Image Analysis in Biology. D.-P. Häder, editor. CRC Press, Boca Raton, FL. pp. 219–249.

Radermacher, M. 1994. Three-dimensional reconstruction from random projections: orientational alignment via Radon transforms. *Ultramicroscopy.* 53: 121–136.

Radermacher, M., T. Wagenknecht, A. Verschoor, and J. Frank. 1987. Three-dimensional reconstruction from a single-exposure, random conical tilt series applied to the 50S ribosomal subunit of *Escherichia coli. J. Microsc.* 146: 113–136.

Radermacher, M., S. Srivastava, and J. Frank. 1992. The structure of the 50S ribosomal subunit from *E. coli* in frozen hydrated preparation reconstructed with secret. *In* Proc. 10th Eur. Congr. on Electron Microscopy. L. Megias-Megias, M.I. Rodriguez-Garcia, E. Rios, and J.M. Arias, editors. Secretariado de Publicaciones de la Universidad de Granada. Granada, Spain. 3:19.

Ryabova, L.A., O.M. Selivanova, V.I. Baranov, V.D. Vasiliev, and A.S. Spirin. 1988. Does the channel for nascent polypeptide exist inside the ribosome? *FEBS Lett.* 226:255–260.

Sezan, M.I. 1992. An overview of convex projections theory and its application to image recovery problems. *Ultramicroscopy.* 40:55–67.

Srivastava, S., A. Verschoor, and J. Frank. 1992. Eukaryotic initiation factor 3 does not prevent association through physical blockage of the subunit–subunit interface. *J. Mol. Biol.* 226:301–304.

Srivastava, S., A. Verschoor, M. Radermacher, R. Grassucci, and J. Frank.

1995. Three-dimensional reconstruction of mammalian 40S ribosomal subunit embedded in ice. *J. Mol. Biol.* 245:461–466.

Stark, H., F. Müller, E.V. Orlova, M. Schatz, P. Dube, T. Erdemir, F. Zemlin, R. Brimacombe, and M. van Heel. 1995. The 70S *Escherichia coli* ribosome at 23 Å resolution: fitting the ribosomal RNA. *Structure.* 3:815–821.

Stöffler, G., R. Bald, B. Kastner, R. Luhrmann, M. Stöffler-Meilicke, and G. Tischendorf. 1980. Structural organization of the *Escherichia coli* ribosome and localization of functional domains. *In* Ribosomes: Structure, Function, and Genetics. G. Chambliss, G.R. Craven, J. Davies, K. Davis, L. Kahan, and M. Nomura, editors. University Park Press, Baltimore, MD. pp. 171–205.

Verschoor, A. 1989. Morpho-structural studies on the eukaryotic ribosome: three-dimensional reconstructions from single-particle electron microscopic specimens. Ph.D. thesis. State University of New York at Albany.

Verschoor, A., and J. Frank. 1990. Three-dimensional structure of the mammalian cytoplasmic ribosome. *J. Mol. Biol.* 214:737–749.

Verschoor, A., J. Frank, T. Wagenknecht, and M. Boublik. 1986. Computer averaged views of the 70S monosome from *Escherichia coli. J. Mol. Biol.* 187: 581–590.

Verschoor, A., N.-Y. Zhang, T. Wagenknecht, T. Obrig, M. Radermacher, and J. Frank. 1989. Three-dimensional reconstruction of mammalian 40S ribosomal subunit. *J. Mol. Biol.* 209:115–126.

Verschoor, A., R. Milligan, S. Srivastava, and J. Frank. 1990. Structural studies on the eukaryotic ribosome. *In* Proc. XIIth Intl. Congr. for Elec. Microsc. (Seattle, 12-17 August, 1990), Vol. I, pp. 506-7. San Francisco, San Francisco Press.

Wagenknecht, T., R. Grassucci, and J. Frank. 1988. Electron microscopy and computer image averaging of ice-embedded large ribosomal subunits from *Escherichia coli. J. Mol. Biol.* 199:137–145.